Computer Assisted Mechanics and Engineering Sciences, 12: 17–30, 2005.

A reduced multi-step integrated oxidation scheme for methane suitable for use into complex reactive flow calculations

Panayiotis Koutmos, Stavros Dimopoulos
Department of Mechanical and Aeronautical Engineering, University of Patras, Patras, Rio 26500, Greece

(Received October 7, 2003)

In Direct or Semi-Direct Numerical Simulations of turbulent reacting flows the exploitation of complex, realistic and detailed chemistry and transport models often results in prohibitive memory and CPU requirements when flows of practical relevance are treated.

The integrated Combustion Chemistry approach has recently been put forward as a methodology suitable for the integration of complex chemical kinetic and chemistry effects into large scale computational procedures for the calculation of complex and practical reacting flow configurations. Through this procedure a reduced chemical kinetic scheme involving only a limited number of species and reactions is derived from a detailed chemical mechanism so as to include major species and pollutants of interest in the main flow calculation. The chemical parameters employed in this integrated scheme i.e. rates, constants, exponents are then calibrated on the basis of a number of constraints and by comparing computations over a range of carefully selected laminar flames so as to match a number of prespecified flame properties such as adiabatic temperatures, selected target species profiles, flame speeds, extinction characteristics. The present work describes such an effort for a commonly used fuel of both fundamental and practical importance, methane. The proposed nine-step scheme involves nine major stable species and in addition to the basic methane oxidation model also includes NO_X production and soot formation submodels.

Keywords: integrated combustion chemistry, reduced chemistry mechanisms, laminar flames, chemical reaction schemes

1. Introduction

The combustion of hydrocarbons for the production of energy is a common and important phenomenon in many engineering applications. In most practical devices, chemical reactions usually take place within and strongly interact with a turbulent flow and the adequate description of the combustion process requires the consideration of a large number of fluid and chemical parameters [1]. On the other hand during the past decade the demand for higher efficiencies, the stringent emission regulations and the need to reduce costs in design and optimization procedures for combustion chambers has prompted the exploitation of Computational Fluid Dynamics methods in support of experimental procedures [2, 3, 4].

Direct or Semi-Direct Numerical Simulations (e.g. DNS, LES) of turbulent reacting flows offer a promising tool toward the understanding of the complex physics of these flows. The full potential and advantages of these techniques can best be realized when sufficiently complex and realistic chemistry and transport models are exploited [5]. Currently computational costs and numerical considerations preclude spatially three-dimensional turbulent simulations with detailed chemistry and transport models in the parameter range of practical interest. Instead judiciously reduced chemical mechanisms that can be employed profitably within DNS or LES and provide a realistic description of appropriate thermochemical parameters are preferred [2, 5, 6].

A number of methodologies have been exploited to simplify a detailed mechanism e.g. the systematic consideration of steady-state and partial equilibrium assumptions leading to skeletal mech-

anisms [6], the analysis and categorization of characteristic chemical time-scales of separate reaction groups [7] and the Integrated Combustion Chemistry (ICC) approach [8], which involves the use of a limited number of judiciously chosen species and reactions with kinetic parameters tuned to match a prespecified number of constraints and flame properties. The ICC approach, alone or in conjunction with other methodologies offers a viable alternative systematic reduction procedure targeting specific requirements with reference both to the thermochemical submodels and to the complete computational procedure. In contrast to the first two approaches, [6, 7], it only involves a limited number of steps and focuses on major species and pollutants of interest for the main simulation in the effort to avoid the burden of intermediate radicals and elementary rates altogether that would prohibitively burden the basic computational procedure.

The present work describes such an effort to derive a simplified and tractable chemical scheme for the oxidation of methane, a fuel of practical interest, including NO_X and soot production models. Its chemical parameters are calibrated by using this scheme within one and two-dimensional reacting flow solvers and by computing a number of well documented one and two-dimensional and coflowing laminar flames, lifted and attached and by matching a number of flame properties such as peak temperatures, major target species, flame speeds and extinction characteristics. The successful derivation and encouraging validation of the presently proposed scheme for methane lends support for an extension of the approach to more complex hydrocarbons, such as propane, ethylene and alternative fuels of practical relevance such as H_2 and CH_3OH.

2. The integrated combustion chemistry methodology

2.1. The basic approach

The proposed approach is based on the requirement that the resulting mechanism must be able to predict to a significant extent what a state of the art multi-step reduced mechanism is predicting for one, two-dimensional and jet flames. The route to achieve this relies on the calibration of the rate parameters of a starting selected chemical scheme by computing laminar flames for which credible experimental data exist. In this investigation the three-step reduced scheme given by Peters and Williams [6] is chosen here as the starting mechanism for the basic methane oxidation:

$$CH_4 + O_2 \rightarrow CO + H_2 + H_2O, \tag{R1}$$

$$CO + H_2O \leftrightarrow CO_2 + H_2, \tag{R2}$$

$$2H_2 + O_2 \leftrightarrow 2H_2O. \tag{R3}$$

The original global rate parameters were given in reference [6] in terms of linear combinations of many of the rates of the elementary reactions of the C_1-chain skeletal mechanism and involved a number of intermediates and radicals. The original basic steps and species of (R1) to (R3) are here retained but the target is to produce global rates with simple kinetic parameters *excluding altogether* intermediate elementary rates and radicals in the resulting global rate expressions.

The framework to achieve this goal has been put forward by [8]. A *first* objective is the prediction of the flame temperature and heat release in various cases. Because no extended product dissociation is allowed the fuel heat of reaction is slightly (5%) reduced to reproduce the experimental temperatures. The *second* objective is the reproduction of the variation of the laminar burning velocity versus mixture dilution as close as possible by regulating the pre-exponential constants (A_k), the activation energies (E_{Ak}) and the species exponents of the above three rates to fit the available experimental data. An appropriate choice of a set of A_k, E_{Ak} and relevant exponents is additionally constrained by the adequate prediction of the extinction limits of selected opposed jet or stagnation point flames. The *third* objective is the adequate computation of targeted product species profiles for a range of strain rate values. This is interrelated with the requirement that the resulting scheme is capable of predicting unsteady effects, an aspect that is particularly significant in highly turbulent

flame calculations and at conditions involving localized extinctions and reignitions. Here a pulsating laminar stagnation point diffusion flame is used for validation.

Apart from the choices for the chemistry model the molecular transport model can also affect the correct computation of the flame properties. As in massive complex flow simulations simplified transport models are frequently exploited, (e.g. [2, 3, 5]), validation tests are here performed utilizing similar levels of complexity. Fick's law with constant Lewis numbers, Sunderland's law for viscocity, constant Prandtl and Schmidt numbers and temperature dependent specific heats were presently employed. Anticipating that radiative losses can have a significant influence on NO_X levels an optically thin radiation model was embodied in the calculations where only CO, CO_2, H_2O and soot (when modeled) emission is considered. The divergence of the net radiative heat flux can be written as:

$$\nabla q_r = C_V f_V T^5 + 4\pi \sum a_{ik} \rho_k I_{bik} \tag{1}$$

where f_V is the soot volume fraction and I_{bik} is the Planck function. The constant C_V is here taken as $4.243{*}10^{-10}$ according to the suggestions of reference [9].

2.2. The proposed mechanism

The basic oxidation of methane is here conveniently represented by the aforementioned three-step scheme of reaction set (R1) to (R3). Regarding the production of NO_X it has been established that the three main routes to NO formation are the prompt, the thermal and the N_2O mechanism while in rich environments the reburn mechanism is also known to be important. Excluding the N_2O contribution the proposed scheme takes into account the remaining contributions through the set of reactions:

$$0.5N_2 + [O] \leftrightarrow NO, \tag{R4}$$

$$0CH_4 + N_2 + O_2 + 0[O] + 0H_2O \leftrightarrow 2NO + 0CH_4. \tag{R5}$$

The required oxygen radical although included in the above reactions, it does not participate explicitly and is conveniently here obtained from partial equilibrium assumptions [6]. The involvement of water and oxygen radicals in the prompt production rate [2, 3] is therefore accounted for in the formulated reduced NO_x reaction scheme. The influence of intermediates and radicals related to the fuel structure is necessarily mimicked through methane, which acts as a catalyst in reaction (R5).

To complete the overall scheme a model for soot formation and oxidation has also been implemented employing many features from the successful soot model proposed by Linstedt [10]. The underlying reactions for acetylene production are here all summed up and represented through one model reaction of the form:

$$2CH_4 \leftrightarrow C_2H_2 + 3H_2. \tag{R6}$$

The corresponding soot nucleation and growth processes are addressed following the modeling assumptions of reference [10] and represented as:

$$C_2H_2 \rightarrow 2C_s + H_2. \tag{R7}$$

The subsequent soot oxidation reactions due to OH radicals and O_2 is here modeled and expressed as:

$$C_s + 0.5O_2 \rightarrow CO, \tag{R8}$$

$$C_s + H_2O \rightarrow CO + H_2. \tag{R9}$$

In line with the integrated concept of the proposed mechanism radicals involved in the original mechanism (e.g. OH, H) have been replaced by stable species (e.g. H_2O, H_2) addressed in the proposed reduced scheme. The resulting soot chemical scheme is implemented and applied by solving two additional transport equations for particle number density and soot mass fraction as discussed below in Sec. 3.

2.3. Determination of global mechanism kinetic rate parameters

An iterative process is employed to determine the kinetic rate parameters A_k, E_{Ak} and any species exponents for each of the above chemical subschemes starting from the basic oxidation section (reactions (R1) to (R3)). With Prandtl and Schmidt numbers fixed to 0.76 and the simplified transport model described previously the kinetic parameters are tuned through a series of test runs involving the prediction of the temperature and species profiles, the flame speed and the extinction behavior of laminar one and two-dimensional and coflowing jet flames within the context of the constraints described in Sec. 2.1. With the methane oxidation scheme established the NO_X reactions ((R4) and (R5)) are then added and similarly tested and tuned with guidance from and reference to several features of the relevant elementary NO_X production steps.

The rate parameters of reaction (R4) are tuned to achieve the correct prediction of thermal NO_X levels and then the prompt (Fenimore) and reburn contributions are apportioned through reactions (R5) in the test cases described in Sec. 4. In an analogous fashion the soot reaction scheme is finally added and the rate constants for reactions (R6) to (R9) are adjusted to reproduce the correct levels of C_2H_2 and soot volume fraction for the test cases selected and reported below. The final set of the kinetic rate parameters is given in Table 1.

Table 1. Specific Reaction Rate Constants for reduced CH_4-air oxidation scheme

Rxn No.	Preexponential (A_k)	Temperature exponent (a_k)	Activation Energy, (E_{Ak})	Species exponents
R1	12.5	0	2185	$CH_4^{0.895}$
R2,f	48750	1.65	−300	$CO^{0.8}$, $H_2O^{1.25}$
R2,b	$1.825*10^6$	1.14	−800	$CO_2^{0.8}$, $H_2^{1.15}$
R3,f	$4.2*10^8$	−0.72	0	$H_2^{1.15}$, $O_2^{0.65}$
R3,b	$1.25*10^8$	−0.7	0	$H_2O^{1.25}$
R4,f	$1*10^{10}$	0.3	37770	$[O]^{0.97}$
R4,b	$1.3*10^7$	0.9	20600	$NO^{0.745}$, $[O]^{1.04}$
R5,f	$4.4*10^9$	0	11100	$CH_4^{0.02}$, $N_2^{1.16}$, $O_2^{0.05}$, $H_2O^{0.5}$
R5,b	$9*10^8$	0	8100	$CH_4^{0.06}$, $NO^{1.42}$
R6,f	$3*10^{21}$	−4.35	24500	
R6,b	$7.5*10^{19}$	−3.8	34500	$C_2H_2^{0.95}$, $H_2^{0.01}$
R7	As reported in [10]	As reported in [10]	23000	$C_2H_2^{0.95}$
R8	As reported in [10]	0.4	23850	As reported in [10]
R9	3.6	0.75	0	$C_S^{0.1}$, $H_2O^{1.725}$

Units in mole/cm^3, sec^{-1}, K, cal/mole. (Species exponents not declared above are unity)

3. The numerical method

The flame configurations studied here are simulated by solving the time-dependent form of the two-dimensional gas-phase conservation equations for reacting flow. The adopted methodology is similar to that of [11] and closely derives from the formulations of [4]. Conservation equations for mass, momentum, energy and species are solved and the equation set can be expressed in Cartesian

coordinates with the general form:

$$\frac{\partial(\rho\phi)}{\partial t}+\frac{\partial(\rho u\phi)}{\partial x}+\frac{\partial(\rho v\phi)}{\partial y}=\frac{\partial}{\partial x}\left(\Gamma_\phi\frac{\partial\phi}{\partial x}\right)+\frac{\partial}{\partial y}\left(\Gamma_\phi\frac{\partial\phi}{\partial y}\right)+S_\phi, \tag{2}$$

ρ, u and v denote density, axial and transverse velocities and depending on the variable used for ϕ (i.e. $1, u, v, H$ or Y_i) this general form represents the conservation of either mass, momentum, energy or species. The transport coefficients Γ_ϕ are obtained from the molecular transport model discussed previously while the source terms are similar to those discussed in [11]. Additionally the state equation,

$$P=\rho R_u T\sum_i\frac{Y_i}{W_i}, \tag{3}$$

where R_u is the universal gas constant, T is the temperature, W_i is the molecular weight of specie i and the net rate of production of the ith species due to the number of chemical reactions N_k expressed as:

$$w_{i,k}=\left(\nu''_{ik}-\nu'_i\right)*A_k*T^{a_k}\exp\left\{-\frac{E_{Ak}}{R_uT}\right\}\prod_{i=1}^{N_k}\left(\frac{\rho Y_i}{W_i}\right)^{\nu_{ik}} \tag{4}$$

which appear in the source terms of the species conservation equations, complete the set of governing equations. Here Y_i is the mass fraction of the specie i, ν''_{ik} and ν'_{ik} are the stoichiometric coefficients of specie i in reaction k in forward and backward direction, ν_{ik} are concentration exponents of specie i involved in reaction step k, A_k and E_{Ak} are the preexponential factor and activation energy in the Arrhenius law of reaction k.

The computational domain is variable in each different test case and is commonly bounded by inflow and outflow boundaries, wall and symmetry or axis planes, where appropriate boundary conditions are applied. The governing equations are integrated by using a finite-volume approach with a staggered, non-uniform grid system. The momentum equations are discretized using an implicit QUICKEST finite-difference scheme (Koutmos et al. [4]), while a hybrid scheme is employed for stability in the species equations. An iterative alternating direction implicit (ADI) technique is used for solving the set of N_s+3 algebraic equations (N_s is the number of species). A stable numerical integration procedure is achieved by coupling the species and energy equations through the chemical reaction source terms and the chemical source terms are linearized to improve convergence. The pressure field is calculated at every time step by solving the pressure Poisson equations in every grid node simultaneously and exploiting the LU (Lower and Upper diagonal) matrix decomposition technique. For the validation test runs involving freely propagating premixed flame configurations the standard PREMIX Sandia code [12] was used. The extinction behavior of non-premixed stagnation point flames to steady and unsteady strain rate were investigated by adapting the basic two-dimensional detailed flow solver to the particular flame/geometry configuration.

The chemical reaction scheme for soot production and oxidation is combined with the solution of two additional model transport equations for particle number density, N_s, and soot mass fraction, Y_s, as proposed by [10], that have the same form as Eq. (1). Chemical reaction (R7) represents here both nucleation and growth while reactions (R8) and (R9) represent the soot oxidation process.

The source term, S_{Ys},for soot mass fraction, Y_s, can then be written:

$$S_{Y_s}=2k_{7,\mathrm{Nucl}}[\mathrm{C_2H_2}]W_s+2k_{7,\mathrm{Growth}}A_s[\mathrm{C_2H_2}]W_s-k_8A_s[\mathrm{O_2}]W_s-k_9A_s[\mathrm{H_2O}]W_s \tag{5}$$

while that for particle number density, N_s, can be expressed as:

$$S_{N_s}=2k_{7,\mathrm{Nucl}}[\mathrm{C_2H_2}]\frac{N_A}{n_{C,\min}}-2C_ad_p^{\frac{1}{2}}\left(\frac{6\sigma_BT}{\rho_s}\right)(\rho N_S)^2\,. \tag{6}$$

According to the recommendations of reference [10] the following set of constants is utilized in the above source expressions. W_s and ρ_s are the molecular weight and density of soot, $\sigma_B = 1.38*10^{-23}$ J/K is the Boltzman constant, $N_A = 6.232*10^{26}$ is the Avogadro number, $C_a = 9$, $n_{C,min} = 60$ and $A_s = \pi\, d_p^2\, \rho\, N_s$ is the particle surface area with d_p the carbon particle diameter. Here the nucleation and growth rate constants used above, $k_{7,Nucl}$ and $k_{7,Growth}$ for reaction (R7), and the oxidation rate constant due to oxygen, k_8, are taken as suggested by [10] with only minor changes as indicated in Table 1, while the rate constant, k_9, due to soot oxidation from OH is duly modified to take into account the replacement of the radical OH contribution in reaction (R9) with the stable available species H_2O. The tuned reaction rate constants for reactions (R6) to (R9) are also given in Table 1.

4. Results and discussion

The performance of the basic oxidation mechanism was evaluated by computing unstretched laminar premixed methane-air flames having different equivalence ratios, ϕ. An important validation parameter is the laminar flame speed, S_L, which was presently calculated and is compared against experimental data from the extended literature (e.g. reference [6]) as a function of φ in Fig. 1a. The predicted lean and stoichiometric part of the S_L curve appears quite satisfactory with a peak S_L of 0.47 m/sec against experimental values in the region 0.39 to 0.41. The rich S_L branch however seems to be overpredicted possibly due to exclusion of intermediate radicals such as H and OH. A means to alleviate this rich branch deficiency is described below through the parameterization of the preexponential factor of reaction (R3) as a function of the local equivalence ratio.

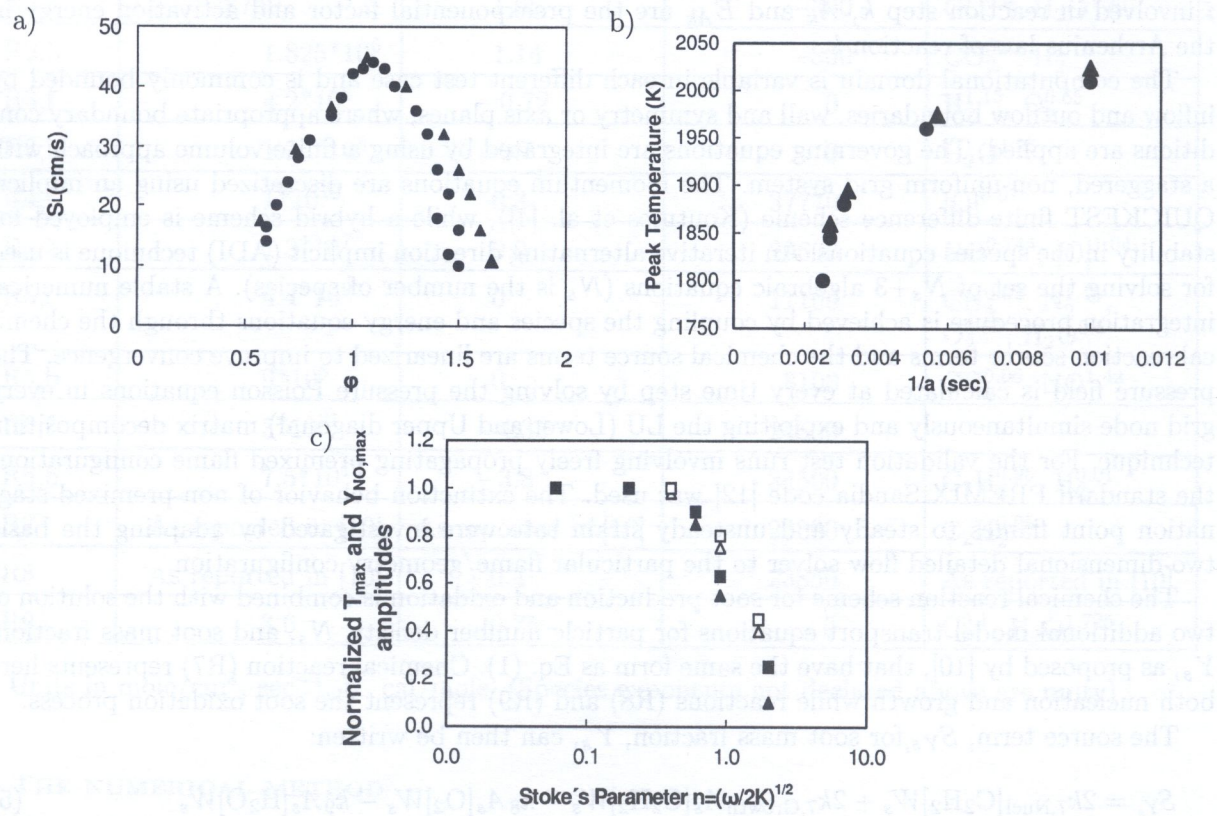

Fig. 1. a) Comparison between computed with the present reduced scheme (▲) and experimental, [6], (•) laminar flame speeds over a range of equivalence ratios for freely propagating premixed flames. b) Peak flame temperatures as a function of the inverse of the strain rate in a stagnation point diffusion flame. Computations of [6] with a four-step reduced mechanism (•), present computations (▲). c) Flame response for a non-premixed stagnation point flame to sinusoidal velocity variations. Open symbols represent current computations, closed symbols computations of [14]. (•, •) Peak temperatures, (•, •) Peak NO concentrations

The reduced scheme (R1) to (R3) was subsequently tested by computing a stagnation point diffusion flame in front of a porous cylinder (Tsuji type burner, [13]) in a one-dimensional calculation by reformulating the detailed mathematical model of Sec. 3. Computed major species and temperature profiles for a strain (a) of 100 $\sec^{-1}$ agreed well with the classical experimental results of Tsuji and Yamaoka [13]. Figure 1b depicts these comparisons and the non-monotonic variation of the peak temperature as a function of $1/a$. As the residence time ($=1/a$) decreases the peak temperature drops due to reactant leakage until no steady state solution exists and this point corresponds to the extinction limit. The computed a_{ex} is 370 $\sec^{-1}$ while the measurements of reference [13] suggested a value of about 330 $\sec^{-1}$. As unsteady effects play an important role during localized extinctions and reignitions in highly turbulent flames unsteady run tests were also performed for a pulsating stagnation point diffusion flame. Egolfopoulos and Cambell [14] have studied the response of such types of flames by imposing sinusoidal variations of strain rate and analyzed the results introducing a new Stokes number, $n = (\omega/2K)^{1/2}$, where ω is the angular frequency ($= 2\pi f$) and K is the strain rate. Unsteadiness has also been known to affect NO_x production rates. Figure 1c compares the normalized amplitudes of the maximum temperature and NO_x mass fraction peak levels versus the Stokes number as calculated from the present scheme (including reactions (R4) and (R5)) against computations produced by reference [8] and obtained with the full GRI 2.11 mechanism. Evidently the presently proposed scheme produces an adequate response to the unsteady strain field as the detailed mechanism used in [8], despite the different levels of the relevant calculated values of temperature and NO_x.

Amongst the extended range of flame configurations tested one selected for discussion here is the counterflow methane-air diffusion flame of Kim et al. [15], where detailed and parametric measurements of major species including acetylene and NO_x levels have been obtained in an effort to study

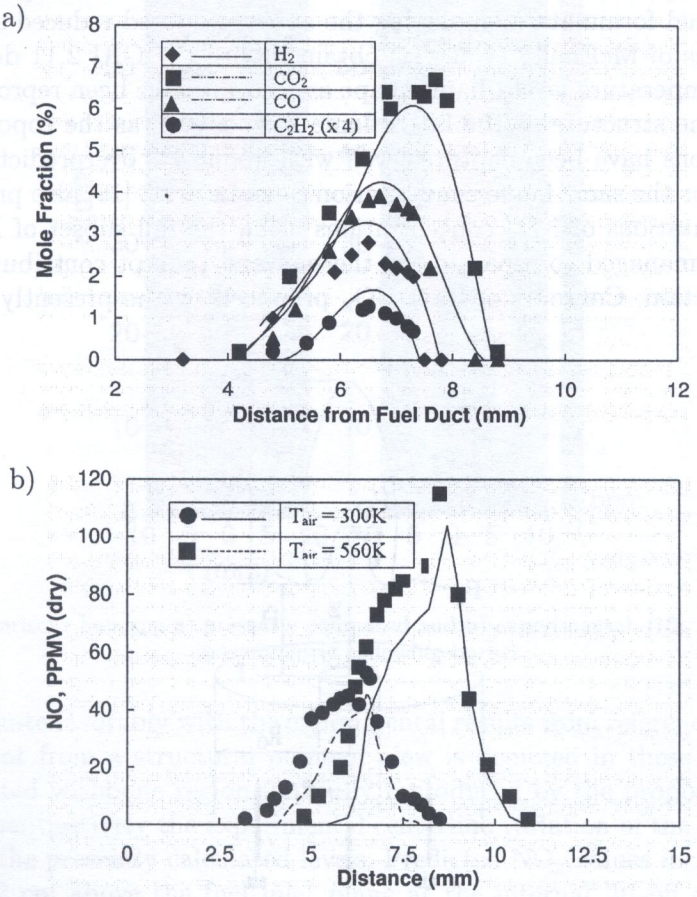

Fig. 2. Comparisons between present calculations (lines) and measurements of [15] (points) in counterflow diffusion flame configuration, a) major species profiles (air preheat 300 K), b) NO_x levels at air preheat of 300 and 560 K

the effects of air preheat on flame structure. The results of the comparisons between the present numerical calculations and the reported measurements in reference [15] are shown in Figs. 2a and 2b. The agreement in major species and acetylene profiles is very good as illustrated in Fig. 2a for an air preheat temperature of 300 K, while a similar level of agreement was obtained for the higher preheat temperature of 560 K (not shown here for brevity). Regarding the total NO_x mole fraction levels, profile comparisons in Fig. 2b for the two preheat temperatures indicate that the qualitative and quantitative agreement achieved by the present chemistry scheme is good. Discrepancies increase at the higher preheat temperature and at the fuel-rich side but the above level of agreement is deemed very reasonable considering the simplifying assumptions involved in the present scheme. Nevertheless, the quite consistent reproduction of the measured trends in NO_x levels with regard to changes in the input parameters (i.e. air preheat) is a very encouraging and valuable attribute of the present model.

Subsequently a range of two-dimensional axisymmetric coflowing laminar jet diffusion flames with or without partial premixing, attached and lifted were calculated targeting the qualitative and quantitative reproduction of major species, temperature, NO_x and soot production. Any discrepancies identified in these test runs led to readjustment of the reduced chemical scheme rate parameters that were fed back to the runs for the one-dimensional flames discussed above; this iterative cycle produced the final tuned set of the chemical rate parameters of Table 1.

A sketch of the two-dimensional axisymmetric geometry burner configuration employed in the two-dimensional computations is given in Fig. 3. It includes a fuel supply, an oxidizer supply and in certain test cases a coflowing surrounding air stream. In the first test case the flame configurations studied by Smooke et al. [16] and McEnally et al. [17] were used for the present computations. Fuel (a mixture of CH_4/N_2 at 0.5149/0.4851 by mass) and air both coflowed at 0.35 m/sec and formed a diffusion flame slightly detached from the burner rim. Temperature isopleths predicted by the present two-dimensional formulation employing the above proposed reduced scheme are compared with the computations of McEnally et al. [17] obtained with the GRI 2.11 detailed mechanism in Fig. 4. Apparently temperature levels, flame shape and height have been reproduced very well. The all important wishbone structure at the lifted flame base as well as the topology of the high and low temperature regions have been captured well with about 4% overprediction of reported peak temperature levels. For the same flame configuration Smooke et al. [16] also provided detailed measurements and computations of NO_x concentrations using the full subset of NO_x reactions in the GRI mechanism and managed to separate the thermal and prompt contributions with respect to the total NO_x production. Contours of total NO_x produced by the presently tuned scheme ((R4)

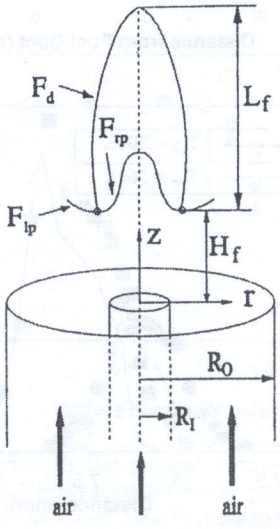

Fig. 3. Unconfined (plane or coflowing) axisymmetric laminar diffusion flame burner configuration

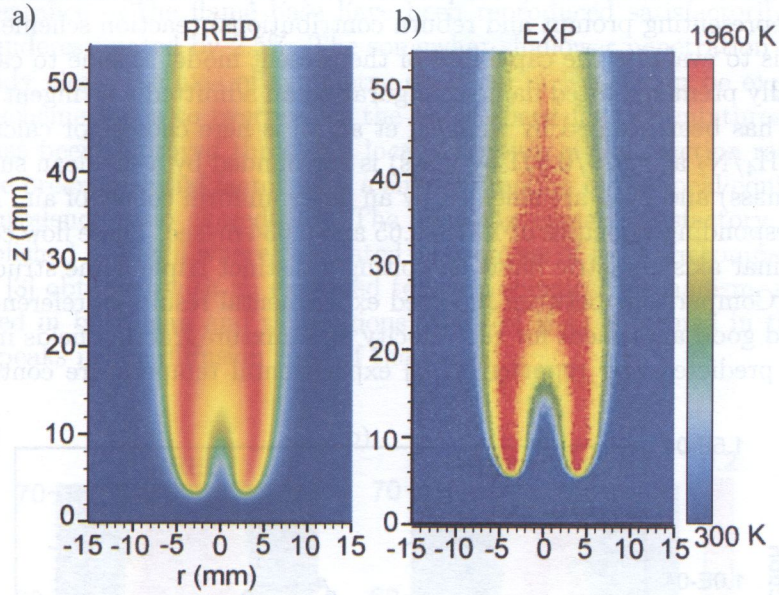

Fig. 4. Computations of temperature isotherms in axisymmetric coflowing burner, a) present reduced scheme, b) McEnally et al. [17] with detailed GRI 2.11 mechanism

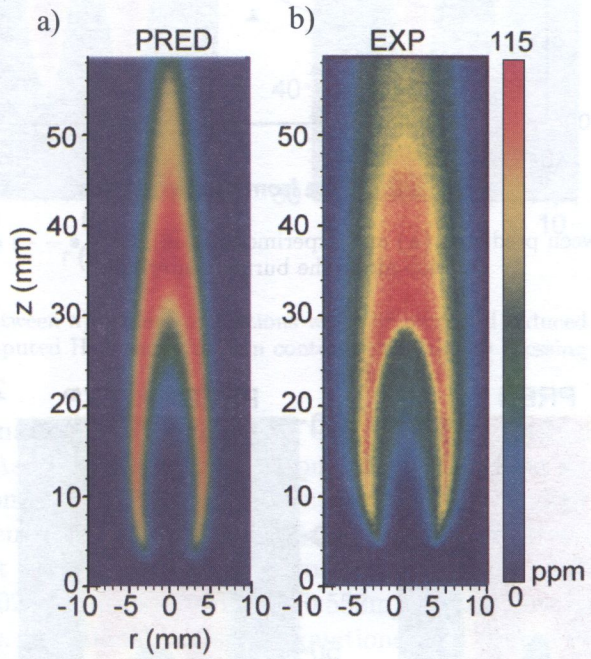

Fig. 5. Comparisons between a) presently computed and b) experimental, [16], NO_x isopleths in axisymmetric coflowing burner

and (R5)) compare quite favorably with the experimental results from reference [16] in Fig. 5. A very satisfactory agreement from a structural point of view is depicted in these comparisons with the characteristic elongated wishbone region faithfully reproduced by the proposed (R4) and (R5) set of reactions. More quantitatively the experimental centerline variation of the total NO_x is displayed in Fig. 6 along with the presently calculated levels. Predicted NO_x values increase along the burner axis and peak at 3.2 cm above the fuel inlet plane at the internal lift-off crevice in accord with the measurements. Computations reported by reference [16] apportioned the relative contribution of ([N_2O+thermal]/[prompt]) in the total NO_x levels at (15/85) for this flame configuration. A very

similar proportion has been achieved by the present (R4) (representing thermal and N_2O contributions) and (R5) (representing prompt and reburn contributions) reaction scheme. The objective of the next test case is to evaluate the capability of the present model scheme to capture the characteristics of a partially premixed lifted flame configuration an admittedly stringent test. A three-feed configuration that has been studied by Plessing et al. [3] is here chosen for calculation. A central fuel rich supply (CH_4/N_2 at 0.679/0.321 by mass) is surrounded by a fuel lean supply (CH_4/Air at 0.0149/0.9851 by mass) and both are shielded by an outer uniform coflow of air. The three streams are flowing at corresponding velocities of 1.178, 0.65 and 0.634 m/sec. These flow conditions produce a highly lifted laminar axisymmetric flame exhibiting a distinct triple flame structure in the stabilization region [3]. Comparisons between reported experimental results in reference [3] and present predictions revealed good agreement for the velocity and mixture fraction fields in the stabilization region. Presently predicted and reported in [3] experimental temperature contours are depicted

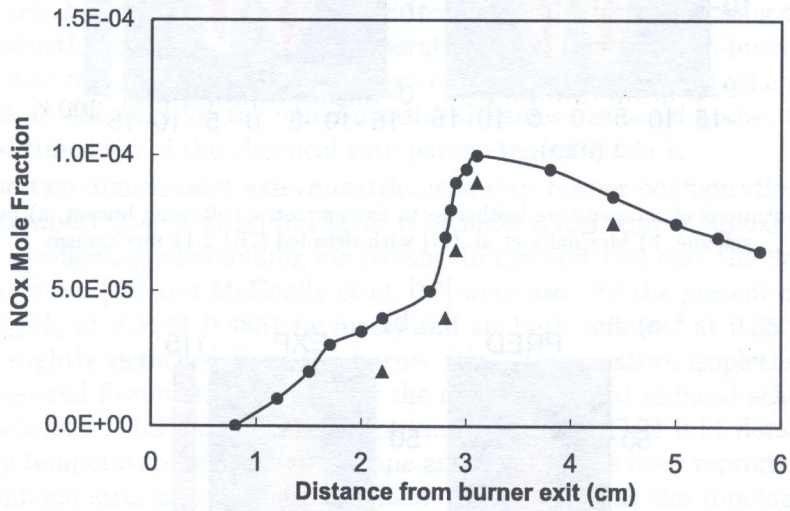

Fig. 6. Comparisons between predicted (▲) and experimental, [16], (– – • – –) distributions of NOx mole fraction along the burner centerline

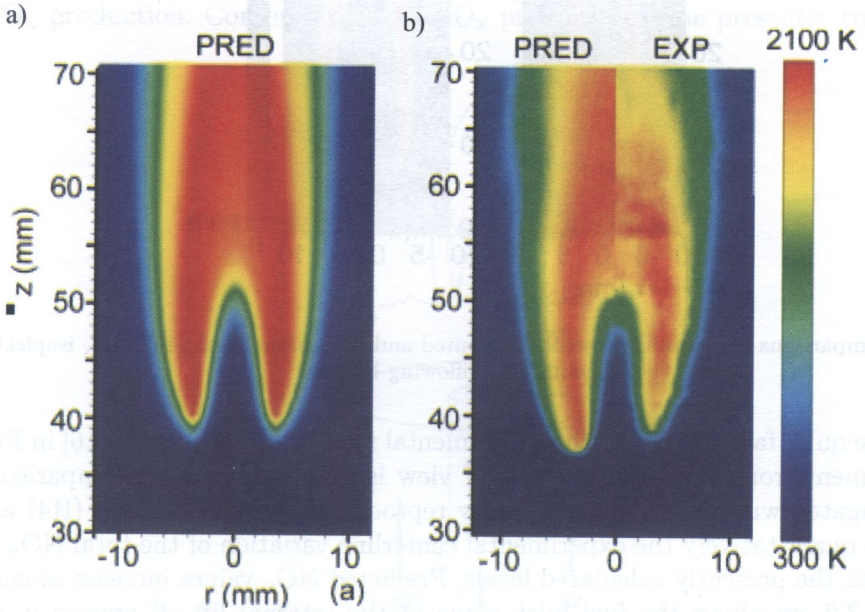

Fig. 7. Comparisons between a) present predictions with the proposed reduced scheme and b) measured and computed temperature distributions reported by Plessing et al. [3]

alongside in Fig. 7 and suggest that temperature distributions, peak levels, flame shapes and the two-tongued appearance of the flame base have been reproduced satisfactorily, while the lift-off height has been underestimated by 2.5%. The somewhat shallower penetration of the unburnt gas into the flame body along the axis of symmetry observed in Fig. 7 can be explained by the fact that the present scheme tends to overpredict the flame speed for rich mixtures as also evidenced in Fig. 1a. This has been improved through a local reduction of the reaction rate of reaction (R3) by multiplying the preexponential factor with a simple function of the local equivalence ratio $G(\phi)$ whenever the equivalence ratio exceeds 1.3. The resulting overall satisfactory prediction for this flame is also established in Fig. 8 where calculated isocontours of H_2O are compared against predictions of reference [3] obtained with an extended ten-step chemical mechanism, signifying the good agreement achieved in both lean and rich regions. Most of H_2O is formed in the rich part of the flame while CO_2 peaks in the diffusion zone of the flame.

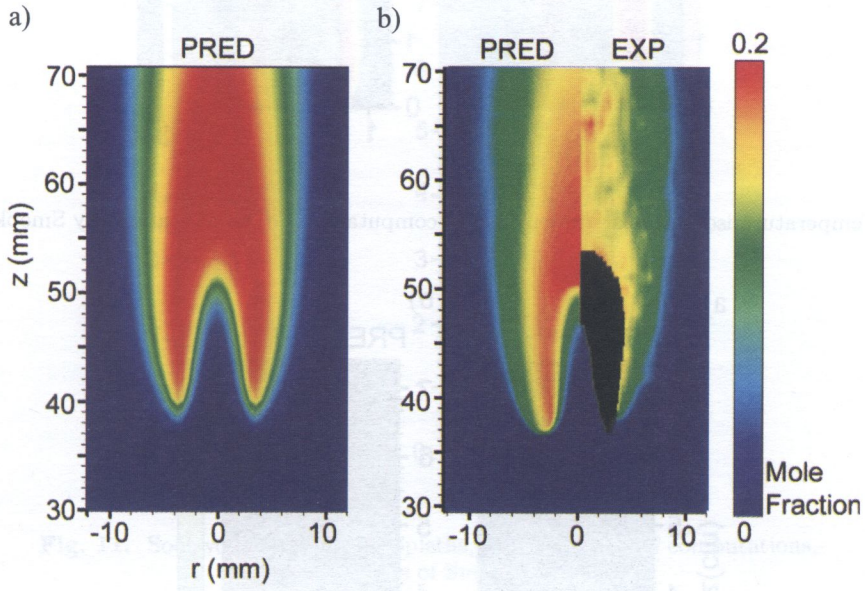

Fig. 8. Comparisons between a) present predictions with the proposed reduced scheme and b) measured and computed H_2O mole fraction contours reported by Plessing et al. [3]

The soot model was finally added to the basic CH_4 oxidation mechanism and tested in a range of flame configurations. As an example calculations of a two-stream axisymmetric sooty laminar coflowing CH_4-air diffusion flame (Fig. 3 type burner) previously studied computationally in detail by Smooke et al. [9] who employed the GRI 3.0 mechanism and an extended multi-step soot scheme are presented in this test case. In the basic burner configuration of Fig. 3, a central supply of fuel (CH_4/Ar at 0.975/0.025 by mass) flowing at 0.552m/sec was now surrounded by oxidizing air coflowing at 0.1254 m/sec. Additional transport equations with source terms given by Eqs. (5) and (6) and reactions (R6) to (R9) were now employed in these computations. Figure 9 demonstrates that the present model predicts the general shape, structure and peak temperature levels of this complex flame configuration. The level of agreement for the major species was of similar good quality as encountered in the previously discussed computations. Within the context of the present reduced scheme, a critical factor in reproducing the measured soot distributions is the adequate reproduction of the acetylene profile concentrations, the only soot precursor addressed in the reduced scheme, since benzene is here excluded. Computed C_2H_2 isopleths are compared in Fig. 10 with the predictions of Smooke et al [9] obtained with a detailed GRI 2.11 mechanism and an extended soot treatment including inception, surface growth, oxidation, and coalescence of soot particles. It is demonstrated that at least for the studied configuration, the level of qualitative and quantitative agreement produced by the simplified reaction model (R6) to (R9) regarding peak C_2H_2 concentrations on the

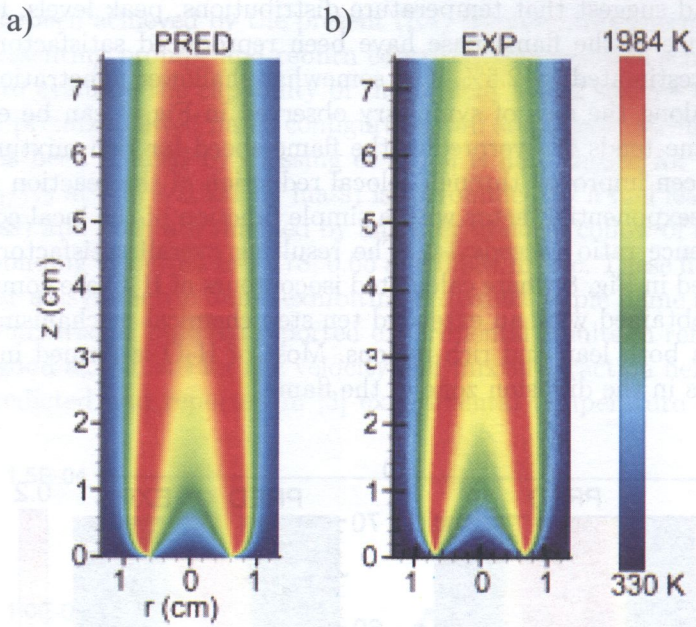

Fig. 9. Temperature isotherms a) present model computations, b) computations by Smooke et al. [9]

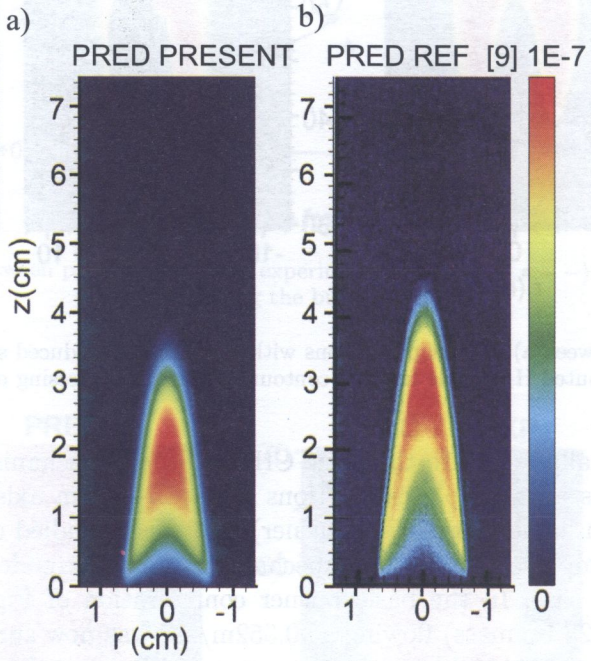

Fig. 10. Acetylene mole fraction distributions, a) present model computations, b) computations of Smooke et al. [9]

center line and disposition of C_2H_2 production and decay zones at the flanks of the flame is rather encouraging. The resultant predicted soot volume fraction contours are plotted in Fig. 11 against the simulated distributions reported by reference [9]. Soot volume fraction topology is captured well and although soot levels are underpredicted in places by about 25% , qualitatively these predictions reveal all major structural features exhibited by the detailed scheme; peak values of soot volume fraction are underestimated by about 5 to 10%.

From the above described test runs and comparisons it appears that the proposed reduced scheme has an acceptable and consistent behavior over the range of flame conditions investigated and ad-

equately predicts the target characteristics of Sec. 2.1 for the diffusion and premixed flame configurations studied. Inaccuracies apparently increase locally for rich mixtures beyond an equivalence ratio of about 1.3 e.g. in the test runs for the lifted flame. This aspect can be conveniently remedied by employing concepts of adaptive chemistry [18] and locally adjusting (at each computational grid node and time-step) selected parameters of the reduced scheme in accordance with the prevailing local flame conditions. Here the flame speed was retarded for rich compositions (i.e. when the mixture strength locally exceeds 1.3) through the parameterization of the preexponential factor of reaction (R3) as a simple function of the local equivalence ratio thus improving the performance of the chemical scheme over the whole range of mixture compositions.

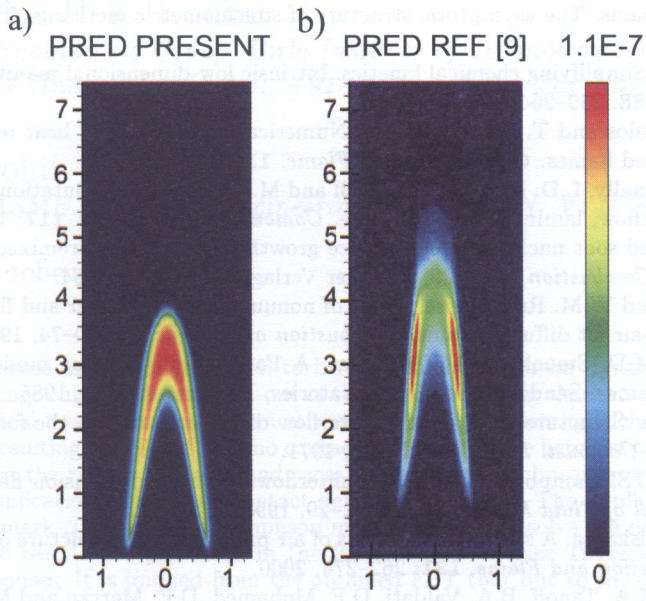

Fig. 11. Soot volume fraction isopleths, a) present model computations, b) computations of Smooke et al [9].

5. Conclusions

An Integrated Combustion Chemistry approach has been employed to derive a reduced oxidation scheme for a technically significant fuel, methane, including submodels for NOx and soot production. The complete scheme involves nine reactions and nine species focusing on major and stable species and pollutants while avoiding altogether the computational burden of intermediate radicals and elementary rates. The chemical rate parameters were calibrated by systematically computing a range of well documented one-dimensional freely propagating, premixed and stagnation point diffusion flames as well as two-dimensional axisymmetric coflowing jet diffusion flames, lifted and attached. Its overall performance has been encouraging and with further tests and refinements it can be valuable in large-scale computations of complex turbulent reacting flows. The procedure can be systematically extended to other practical fuels such as higher hydrocarbons as propane or ethylene or alternative fuels of technological interest such as hydrogen, methanol and ethanol.

Acknowledgments

The research was funded by the "K. Karatheodori" program, Epitropi Ereunon, University of Patras.

References

[1] P.A. Libby and F.A. Williams. *Turbulent Reacting Flows*, Abacus Press, New York, 1993.

[2] D. Haworth, B. Cuenot, T. Poinsot and R. Blint. Numerical simulation of turbulent propane-air combustion with non-homogeneous reactants. *Combustion and Flame.* **121**: 395–422, 2000.

[3] T. Plessing, P. Terhoeven, N. Peters and M.S. Mansour. An experimental and numerical study of a laminar triple flame. *Combustion and Flame.* **115**: 335–353, 1998.

[4] P. Koutmos, C. Mavridis and D. Papailiou. A study of turbulent diffusion flames formed by planar fuel injection into the wake formation region of a slender square cylinder. *Proc. Combust. Inst.* **26**: 161–168, 1996.

[5] W.K. Bushe and R.W. Bilger. Direct numerical simulation of turbulent non-premixed combustion with realistic chemistry. *Annual Research Briefs*, Center for Turbulence Research, NASA Ames/Stanford University; 3–22, 1998.

[6] N. Peters and F.A. Williams. The asymptotic structure of stoichiometric methane-air flames, *Combustition and Flame* **68**: 185–197, 1987.

[7] U. Mass and S.B. Pope. Simplifying chemical kinetics: Intrinsic low-dimensional manifolds in composition space. *Combustion and Flame* **88**: 239–264, 1992.

[8] B. Bedat, F.N Egolfopoulos and T. Poinsot. Direct Numerical Simulations of heat release and NO_X formation in turbulent non-premixed flames. *Combustion and Flame.* **119**: 69–83, 1999.

[9] M.D. Smooke, C.S. McEnally, L.D. Pfefferle, R.J. Hall and M.B. Colket. Computational and experimental study of soot formation in a coflow, laminar diffusion flame. *Combustion and Flame.* **117**: 117–139, 1999.

[10] P.R. Lindstedt. Simplified soot nucleation and surface growth steps for non-premixed flames. In: H. Bockhorn, ed., *Soot Formation in Combustion*, 417–429, Springer Verlag, Heidelberg, 1994.

[11] V.R. Katta, L.P. Goss and W.M. Roquemore. Effect of nonunity Lewis number and finite-rate chemistry on the dynamics of a hydrogen-air jet diffusion flame. *Combustion and Flame.* **96**: 60–74, 1994.

[12] R.J. Kee, J.F. Grcar, M.D. Smooke and J.A. Miller. A Fortran program for modeling steady laminar one-dimensional premixed flames. Sandia National Laboratories, Livenmore, C.A., 1985.

[13] H. Tsuji and I. Yamaoka. Structure analysis of counterflow diffusion flames in the forward stagnation region of a porous cylinder. *Proc. Combust. Inst.* **13**: 723–730, 1971.

[14] F.N. Egolfopoulos and C.S. Campbell. Unsteady counterflowing strained diffusion flames: diffusion-limited frequency response. *Journal of Fluid Mechanics.* **318**: 1–29, 1996.

[15] J. Kim, J. Gore and R Viskanta. A study of the effects of air preheat on the structure of methane/air counterflow diffusion flames. *Combustion and Flame.* **121**: 262–274, 2000.

[16] M.D. Smooke, A. Ern, M.A. Tanoff, B.A. Valdati, D.F. Mohamed, D.F. Marran and M.B. Long. Computational and experimental study of NO in an axisymmetric laminar diffusion flame. *Proc. Combust. Inst.* **26**: 2161–2170, 1996.

[17] C.S. McEnally, L.D. Pfefferle, A.M. Schaffer, M.B. Long, R.K. Mohammed, M.D. Smooke and M.B. Colket. Characterization of a coflowing methane/air non-premixed flame with computer modeling, Rayleigh-Raman imaging and on-line mass spectroscopy. *Proc. Combust. Inst.* **28**: 2063–2070, 2000.

[18] W.H. Green and D.A. Schwer. Adaptive chemistry. *Computational Fluid and Solid Mechanics.* **32**: 1209–1211, 2001.